

Structural and elastic properties of zirconium nitride–aluminum nitride multilayers

W. J. Meng, G. L. Eesley, and K. A. Svinarich*

Physics Department, General Motors Research Laboratories, Warren, Michigan 48090

(Received 30 May 1990)

We have synthesized a series of zirconium nitride–aluminum nitride multilayers with a reactive sputtering technique. Structure and elastic response of these multilayers are characterized by x-ray-diffraction and transient piezoreflectance measurements. We observe a systematic decrease of the longitudinal elastic response in the direction of film growth as the composition modulation wavelength decreases. This contradicts a recent model of the elastic response which predicts the absence of elastic anomaly in metal-insulator multilayers.

Thin films of metal nitrides have received increasing attention for a wide variety of applications ranging from tribology to metallization for microelectronics. While most studies concentrate on preparation, structure, and physical properties of one particular metal nitride, studies on systematic variations of structure and physical properties of multilayered thin films consisting of two different metal nitrides are few in number.^{1,2} The structure and elastic properties of elemental metal multilayers have been extensively studied. Origin of observed changes in elastic response with variation in composition modulation is still a subject of considerable controversy.³ A model has been proposed which relates the observed lattice expansion and elastic anomaly in metal multilayers to charge-transfer effects between adjacent layers.⁴ Absence of the elastic anomaly in metal-insulator multilayers is predicted by this model.

We have synthesized zirconium nitride–aluminum nitride (ZrN/AlN) metal-insulator multilayers using an ultra-high-vacuum (UHV) reactive dc-magnetron sputtering technique. The compositional and structural order of these multilayers are examined by low- and high-angle x-ray diffraction in the symmetrical reflection geometry. A picosecond laser technique is used to measure the longitudinal sound velocity of the multilayers in the growth direction. We show that these multilayers have sharp composition modulation and well-ordered interfaces, that a crystalline to amorphous structural transition occurs around composition modulation wavelength (Λ) of 20 Å, and that there exists a systematic softening of the effective longitudinal elastic constant as Λ is decreased. This softening is similar to that observed in metal-metal systems, and to our knowledge, this is the first such observation in a metal-insulator system.

ZrN/AlN multilayers were grown in a UHV dual-source dc-magnetron sputtering system. The deposition chamber base pressures were kept below 3×10^{-9} Torr for all depositions. A pure Zr (99.9%+) and a pure Al (99.999%+) target were simultaneously sputtered in a mixture of Ar (99.999%+) and N₂ (99.999%+) with individual control of the gas flow rates. Proper adjustment of gas flow rates was crucial for obtaining close to stoichiometric deposition of both ZrN and AlN.⁵ Single-layer ZrN and AlN films and all ZrN/AlN multilayers were grown at the same Ar/N₂ flow rates, which resulted

in a total chamber pressure of 2.70 mTorr. The fluctuation of total chamber pressure is limited to less than 4% by controlling the N₂ flow rate. Both targets were simultaneously presputtered first in Ar and then at the final Ar/N₂ flow rate settings for more than 10 min each. Deposition rates for ZrN and AlN were 3 and 1.8 Å/sec, respectively, and were stable during the whole deposition process. A computer-controlled substrate carrier passed the substrate alternatively over each source. The time substrate spent over each source was controlled to give equal thicknesses of ZrN and AlN individual layers. All films were grown at room temperature on oxidized Si (100) and high-purity fused silica substrates. All multilayers were grown with an equal number of ZrN and AlN individual layers and with AlN in contact with the substrate.

X-ray-diffraction measurements were carried out on a Philips PW1700 automated powder diffractometer equipped with Co *K* α radiation and an exit-beam graphite monochromator. Bulk ZrN is a metal which crystallizes in the cubic NaCl structure whereas bulk AlN is an insulator which crystallizes in the hexagonal Wurtzite structure. X-ray diffraction of single-layer ZrN and AlN films showed cubic and hexagonal patterns. The measured lattice constant for ZrN is $a = 4.661$ Å, for AlN $a = 3.110$ Å, $c = 4.978$ Å. These measured values closely compare with tabulated bulk values.⁶ Single-layer ZrN film did not show strong texturing whereas single-layer AlN film grew with a strong (002) texture. Multilayers grown on oxidized Si (100) and fused silica substrates showed no difference in their x-ray-diffraction patterns.

Figure 1(a) shows the low-angle x-ray-diffraction pattern of a ZrN/AlN multilayer. The low-angle superlattice peaks arise from the electron density modulation in the multilayer, and the peak positions are related to Λ by

$$\left(\frac{n\lambda}{2\sin\theta} \right)^2 = \Lambda^2 \left[1 - \frac{2\delta}{\sin^2\theta} \right], \quad (1)$$

where δ is the average refractive-index deviation from unity and n is the order of the low-angle peak.⁷ The data shown in Fig. 1(a) is analyzed according to Eq. (1) and the result is plotted in Fig. 1(b). Low-angle diffraction measurements were made on a series of ZrN/AlN multilayers and a linear regression of the data yields both Λ

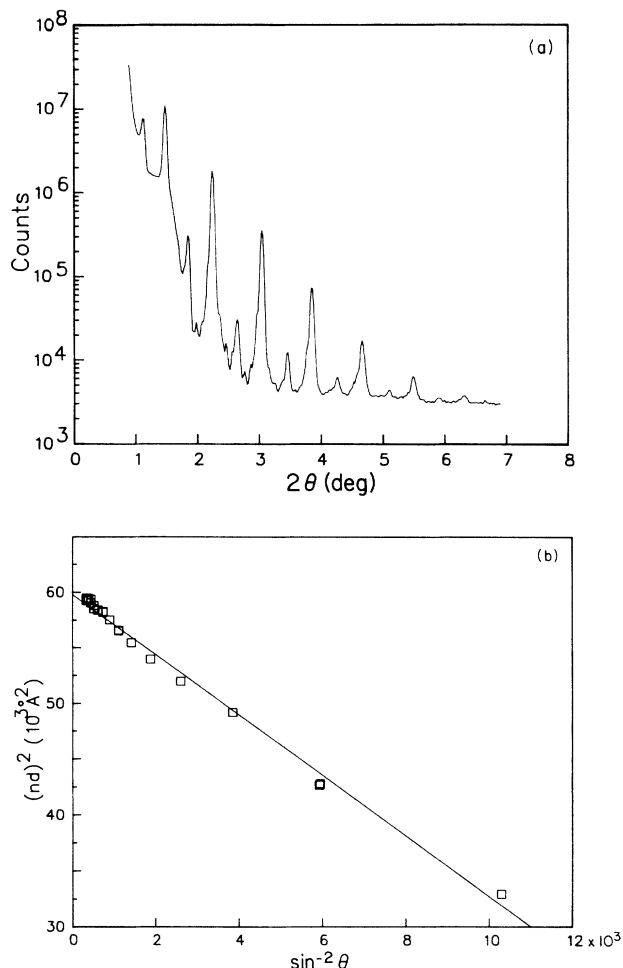


FIG. 1. (a) Low-angle diffraction pattern of a ZrN/AlN multilayer; (b) linear regression analysis of low-angle diffraction data, overlapping data points indicate repeat measurements.

and δ . Table I shows the regression results on all multilayers. Since the low-angle superlattice peaks result from electron density modulation which can be represented by a Fourier expansion, a characteristic interface sharpness can be estimated by $\Lambda/4n_{\max}$, where n_{\max} is the highest order of the observed low-angle peaks.⁸ It is evident from Table I that sharp composition modulation exists for all

multilayers studied. The total film thickness is obtained by multiplying Λ and the number of bilayers in the multilayer.

Figure 2 shows the high-angle x-ray-diffraction patterns for the same series of ZrN/AlN multilayers. Satellite peaks cannot be resolved for the $\Lambda = 245$ Å sample. Two of the three diffraction peaks can be indexed to the (111) and (200) reflections of ZrN, and the only other observed reflection can be indexed to the (002) reflection of AlN. Thus AlN is strongly textured with its c axis in the growth direction, in agreement with what is observed in the single-layer AlN film. The ZrN (111) reflection of the $\Lambda = 245$ Å sample is much more intense than that of (200), whereas they are equally intense in the single-layer ZrN film. It thus appears that the (002) texturing of AlN is forcing a strong (111) texture on to the next ZrN layer. Better lattice matching is achieved because of the same in-plane hexagonal symmetry of ZrN and AlN in this orientation. The in-plane lattice mismatch between ZrN (111) and AlN (002), assuming bulk lattice constants, is 4%.⁶ As Λ decreases to 164 Å, high-angle satellite peaks around ZrN (111) and AlN (002) reflections can be resolved. For Λ ranging between 71 and 29 Å, the high-angle diffraction peaks correspond to the average lattice spacing of ZrN (111) and AlN (002) plus a series of satellite peaks. It is well known that the position of the m th-order satellite peak moves with Λ according to,

$$\frac{1}{d_m} = \frac{1}{d_0} \pm \frac{m}{\Lambda}, \quad (2)$$

where d_0 is the average lattice spacing and d_m is the apparent spacing of the m th-order peak.⁸ Table I shows Λ obtained from high-angle diffraction according to Eq. (2) which shows good agreement between low- and high-angle measurements. The average lattice spacings of ZrN (111) and AlN (002) in the growth direction d_0 for this series of multilayers are also shown in Table I. It is of interest to point out that, although the bulk in-plane mismatch between ZrN and AlN is 4%, d_0 does not change more than 0.4% as Λ is varied. This behavior is different from metallic multilayers where a much larger lattice expansion due to similar in-plane mismatch is expected. As Λ is further decreased from 29 to 16 Å, the high-angle diffraction pattern shows clearly a crystal to amorphous structural transition. A strong low-angle su-

TABLE I. Results of structure and elastic property measurements on ZrN/AlN multilayered thin films. Λ_l and δ are obtained from linear regression of low-angle x-ray-diffraction data. n_{\max} is the highest order of observed low-angle peaks. Λ_h and d_0 are obtained from high-angle x-ray-diffraction data. v is the measured longitudinal sound velocity (see text).

Λ_l (Å)	δ	n_{\max}	Λ_h (Å)	d_0 (Å)	v ($\pm 5\%$) (m/sec)
245(4)	$2.3(1) \times 10^{-5}$	15	...	2.595(1)	8909
164(4)	$2.6(1) \times 10^{-5}$	11	156(5)	2.598(1)	9111
71(2)	$3.4(2) \times 10^{-5}$	5	71(1)	2.599(1)	8606
59(2)	$2.3(4) \times 10^{-5}$	3	59(2)	2.591(1)	8429
38(1)	$3.7(4) \times 10^{-5}$	3	38(1)	2.595(1)	8140
29(1)	$2.2(4) \times 10^{-5}$	3	29(1)	2.597(1)	7660
16(1)	$6(2.5) \times 10^{-5}$	2	8727

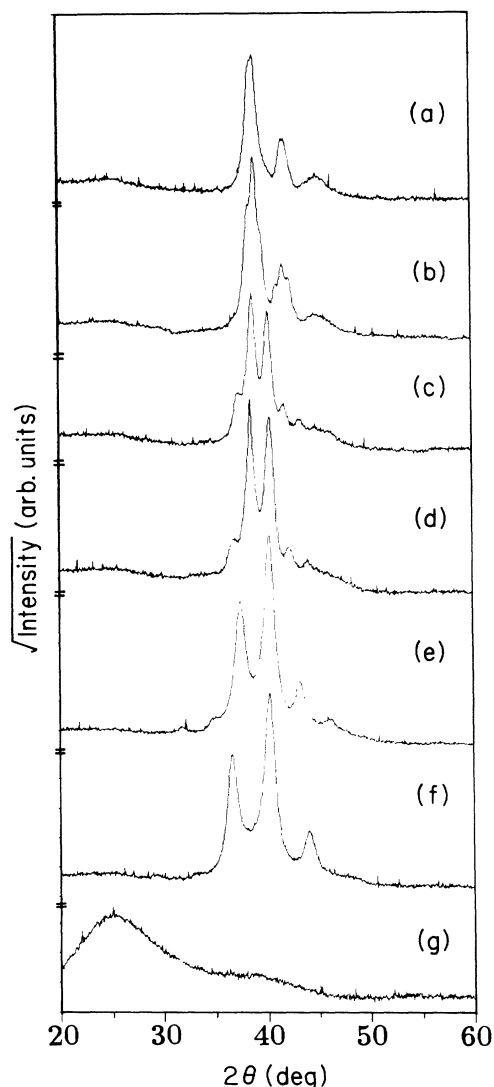


FIG. 2. High-angle diffraction patterns of ZrN/AlN multilayers on oxidized silicon substrates: (a) $\Lambda = 245$ Å, (b) $\Lambda = 164$ Å, (c) $\Lambda = 71$ Å, (d) $\Lambda = 59$ Å, (e) $\Lambda = 38$ Å, (f) $\Lambda = 29$ Å, and (g) $\Lambda = 16$ Å. The diffraction pattern of the $\Lambda = 16$ Å sample on fused silica substrate is shown.

perlattice peak is observed in the $\Lambda = 16$ Å sample, indicating the presence of significant composition modulation. Although such crystal to amorphous structural transitions are commonly observed in metallic multilayers with significant in-plane lattice mismatch, to our knowledge, this is the first such observation made in nitride multilayers.

Longitudinal sound velocities of ZrN/AlN multilayers in the growth direction were measured by a time-resolved transient piezoreflectance (TPR) technique.⁹ A picosecond laser pulse incident upon the film surface generates a longitudinal acoustic pulse in the growth direction into the film. The successive echo pulses reflected from the film-substrate interface back to the surface are detected by measuring the strain-induced reflectivity change. TPR measurements on all ZrN/AlN multilayers revealed that the reflectivity change due to the acoustic pulse echos is small for all multilayers. Since Hf is known to have a

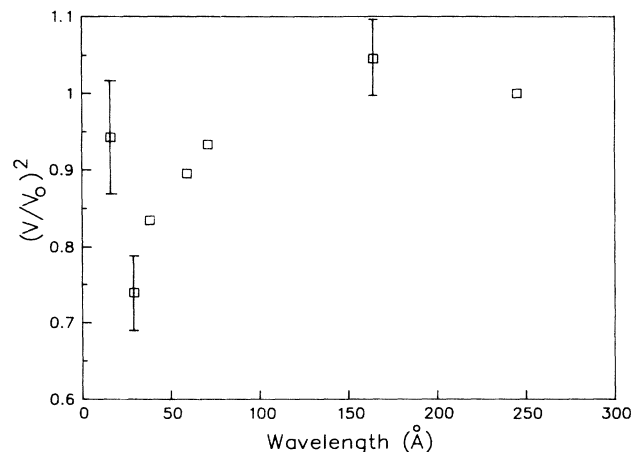


FIG. 3. Square of normalized longitudinal sound velocity in the growth direction vs composition modulation wavelength.

large piezoreflectance response, the magnitude of the reflectance change in the TPR measurements is greatly increased by depositing a layer of Hf on top of all the multilayers. To minimize the Hf thickness variation, Hf was deposited onto all multilayers at once, and Hf was simultaneously deposited onto four bare substrates which surrounded all ZrN/AlN samples during deposition. TPR measurements on these four Hf coated bare substrates yielded identical pulse transit times, indicating negligible Hf thickness variation within the measurement accuracy. The pulse transit time due to the Hf cap was subtracted from the measured total pulse transit times on all Hf-coated ZrN/AlN multilayers to yield the pulse transit times through the multilayers. The longitudinal sound velocities are obtained from dividing twice the total film thicknesses by the pulse transit times, the values of which are also shown in Table I. Figure 3 shows the longitudinal sound velocity squared and normalized to that of the highest modulation wavelength sample ($\Lambda = 245$ Å). With average density of the films fixed, Fig. 3 shows the systematic decrease of the effective longitudinal elastic constant C in the growth direction.¹⁰ The final increase of C at $\Lambda = 16$ Å corresponds to the crystal to amorphous structural transition as shown in Fig. 2. Taking the average film density to be 5.3 g/cm^3 (the average of ZrN and AlN bulk densities), we obtain $C = 4.2 \times 10^{12} \text{ dyne/cm}^2$ for the $\Lambda = 245$ Å multilayer. The decrease of C shown in Fig. 3, follows closely a $1/\Lambda$ dependence. To our knowledge, this is the first observation of a $1/\Lambda$ softening of the effective longitudinal elastic constant in nitride metal-insulator multilayers.

A recent model relates lattice expansion and elastic anomaly in metal multilayers to electric charge transfer between adjacent metal layers. The electrostatic energy of the interface dipole layer has been shown to be inversely proportional to the sum of the Thomas-Fermi screening lengths of the individual constituents. It is argued that a uniform lattice expansion occurs to minimize this electrostatic energy and results in a change of elastic constants.⁴ Since the sum of screening lengths is much larger if one constituent is an insulator, this model predicts the absence

of elastic constant changes in metal/insulator multilayers. We believe our experimental results (shown in Fig. 3) are inconsistent with this model. A similar softening of the effective longitudinal elastic constant in metallic multilayers has previously been observed, and interpreted in terms of weakened interfacial bonding.¹⁰ Our present observations are not inconsistent with such an interpretation.

In summary, we have synthesized ZrN/AlN multilayered thin films with a high degree of compositional and structural order. A crystalline-to-amorphous structural

transition occurs in ZrN/AlN multilayers as Λ decreases from 29 to 16 Å. We observe in these films a systematic softening of effective longitudinal elastic constant in the film growth direction, which contradicts a recent model of elastic response in metal multilayers based on charge-transfer effects. The observed softening is inversely proportional to the composition modulation wavelength. This work points to the need for more systematic investigations of structural and physical property changes in metal nitride multilayers.

*Present address: Physics Department, Wayne State University, Detroit, MI 48201.

¹J. M. Murduck, J. Vicent, I. K. Schuller, and J. B. Ketterson, *J. Appl. Phys.* **62**, 4216 (1987).

²R. Bhadra, M. Grimsditch, J. Murduck, and I. K. Schuller, *Appl. Phys. Lett.* **54**, 1409 (1989).

³R. C. Cammarata, *Scr. Metall.* **20**, 479 (1986).

⁴M. L. Huberman and M. Grimsditch, *Phys. Rev. Lett.* **62**, 1403 (1989).

⁵W. J. Meng (unpublished).

⁶L. E. Toth, *Transition Metal Carbides and Nitrides* (Academ-

ic, New York, 1971).

⁷P. F. Miceli, D. A. Neumann, and H. Zabel, *Appl. Phys. Lett.* **48**, 24 (1986).

⁸D. B. McWhan, in *Synthetic Modulated Structures*, edited by L. L. Chang and B. C. Giessen (Academic, Orlando, 1985), p. 43.

⁹G. L. Eesley, B. M. Clemens, and C. A. Paddock, *Appl. Phys. Lett.* **50**, 717 (1987).

¹⁰Bruce M. Clemens, and Gary L. Eesley, *Phys. Rev. Lett.* **61**, 2356 (1988).